Frontiers in Bioscience Landmark

Front. Biosci. (Landmark Ed) **2026**; 31(9): 55463
https://doi.org/10.31083/FBL55463

Original Research

Proteomic Signatures of Cardiac Mitochondrial Remodelling During Acute Diabetes Reflect Metabolic and Redox Adaptations

Natália Andelová[1], Dávid Janko[1], Milan Zvarík[2], Iveta Waczulíková[2], Simona Papežíková[1], Veronika Farkašová[1], Táňa Ravingerová[1], Miroslav Ferko[1,*]

[1]Institute for Heart Research, Centre of Experimental Medicine of the Slovak Academy of Sciences, 841 04 Bratislava, Slovakia
[2]Department of Nuclear Physics and Biophysics, Faculty of Mathematics, Physics and Informatics, Comenius University Bratislava, 814 99 Bratislava, Slovakia
*Correspondence: usrdmife@savba.sk (Miroslav Ferko)
Academic Editor: Ioanna-Katerina Aggeli
Submitted: 30 June 2026 Revised: 16 August 2026 Accepted: 3 September 2026 Published: 20 September 2026

Abstract

Background: Mitochondria play a central role in cardiac energy metabolism and dynamically adapt to changes in metabolic demand. However, the early mitochondrial adaptations accompanying the acute phase of diabetes mellitus remain insufficiently understood. This study aimed to characterise diabetes-induced mitochondrial remodelling in the rat heart. **Methods:** Diabetes was induced using an established streptozotocin-induced rat model. Cardiac mitochondrial proteomes were analyzed by liquid chromatography–tandem mass spectrometry (LC-MS/MS) in control and diabetic animals. Differential protein abundance was assessed by statistical comparison between groups using the *limma* package in R, and machine learning classification was used to identify proteins with the strongest discriminatory power between control and diabetic states. **Results:** Diabetes was associated with distinct mitochondrial proteomic remodelling. In the diabetic group, monoamine oxidase A (AOFA, p_{adjust} = 0.003) was markedly upregulated, fatty acid β-oxidation-related enzymes including dienoyl-CoA isomerase (ECH1, p_{adjust} < 0.001) and dienoyl-CoA reductase (DECR, p_{adjust} = 0.003) showed increased abundance, and respiratory chain complex I components, particularly NADH-ubiquinone oxidoreductase 75 kDa subunit (NDUS1, p_{adjust} = 0.016) and NADH dehydrogenase [ubiquinone] iron-sulfur protein 2 (NDUS2, p_{adjust} = 0.016), were elevated. Machine learning analysis consistently identified AOFA and key metabolic proteins as the strongest discriminators between diabetic and control animals (n = 6 per group). These changes indicate a coordinated shift towards enhanced lipid utilisation, altered mitochondrial respiratory function, and involvement of redox-associated processes. **Conclusions:** The observed proteomic changes may reflect early adaptive and compensatory mechanisms supporting mitochondrial function under increased energetic and oxidative load and highlight pathways that may represent promising candidates for targeted therapeutic modulation in diabetic cardiac dysfunction.

Keywords: heart; mitochondria; proteomics; machine learning; diabetes mellitus; metabolic reprogramming; fatty acid β-oxidation; monoamine oxidase A

1. Introduction

The heart is able to increase its resistance to injury via induction of intrinsic adaptive mechanisms. In response to increased energy demand, the myocardium activates endogenous cardioprotective pathways involving metabolic adaptation, mitochondrial regulation, and anti-inflammatory signalling, which help preserve cardiac function and limit structural damage [1]. One of the well-established strategies based on these adaptive responses is the phenomenon called preconditioning — a form of "cellular pretraining" that engages complex protective mechanisms [2]. Interestingly, several studies have demonstrated that the early diabetic myocardium exhibits reduced susceptibility to ischaemia–reperfusion injury (IRI), reflecting a balance between metabolic stress and activation of intrinsic protective pathways [3,4,5,6]. At the mitochondrial level, diabetic hearts maintain coupling of oxidative phosphorylation [7,8] and exhibit reduced oxidative damage during IRI [9,10]. They also display increased mitochondrial membrane fluidity, suggesting a signalling role for reactive oxygen species (ROS) in the early adaptive response [9,11]. Furthermore, diabetic mitochondria show increased resistance to calcium overload through modulation of the mitochondrial permeability transition pore (mPTP) [12].

Collectively, these mitochondrial adaptations support the concept that acute diabetes induces a transient mitochondria-mediated adaptive phenotype resembling preconditioning-like cardioprotection [7].

Despite these well-documented functional adaptations, the underlying molecular mechanisms remain incompletely understood. In particular, while alterations in mitochondrial respiration and redox balance have been described, a comprehensive characterisation of mitochondrial protein remodelling during the early phase of diabetes is still lacking. A deeper understanding of these early mitochondrial adaptations may provide novel insights into mechanisms that could be exploited for targeted therapeutic intervention in diabetic cardiac conditions. In diabetic my-

ocardium, oxygen availability is generally preserved; however, mitochondrial utilisation of oxygen is impaired due to disturbances in the respiratory chain. This condition, often referred to as pseudohypoxia, mimics mild hypoxia without a significant reduction in tissue oxygen levels [13,14]. Pseudohypoxia is often associated with hyperglycaemia and is characterised by an increased nicotinamide adenine dinucleotide, reduced/oxidised form ($NADH/NAD^+$) ratio [15]. Our previous research demonstrated that although oxidative phosphorylation remains coupled in diabetic mitochondria, electron transport is slowed and respiratory efficiency is reduced when substrates such as succinate or glutamate are utilised [7].

While our previous studies primarily characterised functional mitochondrial adaptations during acute diabetes and included targeted proteomic analysis of selected proteins associated with the mPTP, the present study extends this work by applying broader liquid chromatography–tandem mass spectrometry (LC–MS/MS)-based mitochondrial proteomic profiling integrated with a machine learning-based analytical framework. This approach enables the identification and prioritisation of proteins according to their discriminatory power, while subsequent functional enrichment and pathway analyses provide insight into the biological processes associated with these discriminating proteins.

Accordingly, in the present study, we aimed to further elucidate mitochondrial adaptations in the acute phase of diabetes and to identify key proteins and pathways associated with early mitochondrial remodelling. By combining differential expression analysis with machine learning (ML), we sought to identify the most relevant discriminating features of the diabetic condition and characterise the biological processes in which these proteins are involved. In addition, we assessed selected antioxidant enzymes and markers of oxidative damage to further evaluate metabolic and redox-related mechanisms contributing to mitochondrial adaptation. Together, this integrated approach aims to provide molecular insight into the mitochondrial remodelling associated with the early diabetic phenotype and to identify candidate proteins and pathways for subsequent targeted investigation.

2. Materials and Methods

2.1 Experimental Animals

Experiments were conducted on male Wistar rats (Dobrá Voda, Slovak Republic) aged 12–15 weeks. A total of 12 animals were included in the study and randomly allocated to the control (n = 6) and diabetic (n = 6) groups. The animals were housed under standard conditions with a 12 h light/12 h dark cycle, at a constant ambient temperature of 22 ± 2 °C and relative humidity of 55 ± 10%. They had unrestricted access to water and were fed a standard pellet diet *ad libitum*.

The study was performed in accordance with the Principles of Laboratory Animal Care established by the Ethical Committee of the Centre of Experimental Medicine of the Slovak Academy of Sciences (CEM SAS), approved by the Animal Health and Animal Welfare Division of the State Veterinary and Food Administration of the Slovak Republic (permit No. Ro 3754/18-221/3), and conducted in compliance with the European Union Directive 2010/63/EU on the protection of animals used for scientific purposes. The study was reported in accordance with the ARRIVE (Animal Research: Reporting of *In Vivo* Experiments) guidelines.

2.2 Induction of Diabetes Mellitus

Diabetes mellitus (D) was induced by a single intraperitoneal injection of streptozotocin (STZ; Cat. No. S0130; Sigma-Aldrich, St. Louis, MO, USA) at a dose of 65 mg/kg body weight, dissolved in 0.1 M citrate buffer (pH 4). The development of diabetes was monitored daily by assessment of glycosuria using GlukoPHAN test strips (Pliva–Lachema, Czech Republic). Animals were maintained in the diabetic state for 7 days, with the experimental endpoint occurring on day 8 after STZ administration. This one-week period represents the acute phase of STZ-induced diabetes, consistent with previously established experimental models [16].

At the end of the experimental period, body weight was recorded, and blood glucose, cholesterol, and triacylglycerol levels were measured using blood collected from the tail vein with a MultiCare analyser and the corresponding test strips (Biochemical Systems International, Florence, Italy). Serum insulin levels were determined using a radioimmunoassay (RIA) kit (Linco Research, USA). The diabetic state was confirmed by the metabolic and biochemical characteristics presented in Table 1, including significantly elevated blood glucose, triacylglycerol, and cholesterol levels and decreased insulin levels compared with age-matched controls, consistent with our previous studies [5,7,12].

Table 1. Metabolic parameters and body weight of control and diabetic rats.

Parameter	Control	Diabetes
Glucose (mmol L^{-1})	6.84 ± 0.22	26.16 ± 1.64**
Triacylglycerol (g L^{-1})	1.39 ± 0.11	5.09 ± 0.31**
Cholesterol (mmol L^{-1})	1.82 ± 0.13	2.62 ± 0.18*
Insulin (ng mL^{-1})	1.19 ± 0.09	0.42 ± 0.06**
Body weight (g)	360 ± 7	314 ± 16*

All values are presented as the mean ± standard error of the mean (SEM), n = 6 per group. Statistical significance was assessed using an unpaired Student's *t*-test: * $p < 0.05$, ** $p < 0.01$.

2.3 Administration of Anaesthesia

Thiopental (Thiopental, VUAB 1.0 g; VUAB Pharma a.s., Czech Republic) was prepared as a 100 mg/mL stock solution and administered intraperitoneally at a dose of 50–60 mg/kg body weight to induce deep anaesthesia, together with heparin (HEPARIN LÉČIVA, 5000 IU/mL; Zentiva, k.s., Prague, Czech Republic) at a dose of 500 IU. The animals were allowed to stabilise for 30 min. While under deep anaesthesia, the hearts were excised for subsequent mitochondrial isolation. Heart excision constituted the terminal procedure and resulted in death.

2.4 Isolation of Cardiac Mitochondria

Cardiac mitochondria were isolated via differential centrifugation at 4 °C. After excision, the hearts were immediately cleaned of surrounding fat and connective tissue and then rinsed with cooled saline. The tissue was placed into isolation buffer I (180 mM KCl, 4 mM EDTA, and 1% BSA in distilled water; pH 7.4, adjusted with Tris/HCl and cooled to 4 °C) and homogenised using the GentleMACS Octo Dissociator with Heaters (Miltenyi Biotec GmbH, Bergisch Gladbach, Germany) (2 cycles, 1 min each). The homogenate was diluted to a total volume of 20 mL with the same isolation buffer and further homogenised manually. The sample was centrifuged at 1000 ×g for 10 min. The resulting supernatant was then centrifuged again at 6200 ×g for 10 min. The pellet was resuspended in cold isolation buffer II (180 mM KCl and 4 mM EDTA in distilled water; pH 7.4, Tris/HCl; cooled to 4 °C) and centrifuged again at 6200 ×g for 10 min. The resulting mitochondrial pellet was resuspended in a small volume of isolation solution without BSA and homogenised [17]. The concentration of proteins in the mitochondrial fraction was determined by a Synergy H1 multidetection reader (BioTek Instruments, Inc., Winooski, VT, USA) using the Bradford method [18]. The purity of mitochondrial fractions prepared using this isolation procedure has been previously validated [19].

2.5 Proteomic Analysis by nanoLC–MS/MS

Mitochondrial samples containing 250 µg of protein were dried in a CentriVap DNA Vacuum Concentrator (Labconco Corporation, Kansas City, MO, USA) and resuspended in 8 M urea (Cat. No. 1.08487; Merck KGaA, Darmstadt, Germany) and 100 mM NH_4HCO_3 (Cat. No. A6141; Sigma-Aldrich, St. Louis, MO, USA) to achieve a final urea concentration of 6.4 M. Proteins were reduced by adding dithiothreitol (DTT; Cat. No. 1.11474; Merck KGaA, Darmstadt, Germany) to a final concentration of 5 mM and incubated for 30 min at 56 °C. Subsequently, proteins were alkylated with iodoacetamide (IAA; Cat. No. I1149; Sigma-Aldrich, St. Louis, MO, USA) at a final concentration of 15 mM for 20 min in the dark at room temperature. The alkylation reaction was quenched by adding DTT to a final concentration of 5 mM. The urea concentration was then reduced to 1.4 M by dilution with 100 mM NH_4HCO_3. Proteins were digested with trypsin (Cat. No. T6567; Sigma-Aldrich, St. Louis, MO, USA) at a 1:25 enzyme-to-substrate ratio (trypsin concentration, 0.2 µg/µL) overnight at 37 °C. The following day, formic acid (Cat. No. 5.33002; Merck KGaA, Darmstadt, Germany) was added to a final concentration of 1%, after which the samples were sonicated and centrifuged at 14,000 ×g. Prior to LC–MS/MS analysis, the resulting peptide samples were desalted using Strata C18-U solid-phase extraction (SPE) columns (Part No. 8B-S002-EAK; Phenomenex, Torrance, CA, USA), according to our previously established protocol [20]. Proteomic analysis was performed using an Ultimate 3000 RSLC nanoLC system (Thermo Fisher Scientific, Germering, Germany) coupled via electrospray ionisation (ESI) to an Amazon SL mass spectrometer equipped with a 3D ion-trap mass analyser (Bruker, Bremen, Germany). Mobile phase A consisted of 0.1% formic acid in 2% acetonitrile (ACN; Cat. No. 1.00029; Merck KGaA, Darmstadt, Germany), and mobile phase B consisted of 0.1% formic acid in 95% ACN. The loading phase consisted of 0.05% formic acid in 2% ACN. Samples were maintained in the autosampler at 4 °C, and an amount corresponding to 4 µg of protein digest was injected for each analysis. Peptides were separated on a C18 Acclaim PepMap column (Thermo Scientific, Waltham, MA, USA; 75 µm × 300 mm, 3 µm particle size, 100 Å) maintained at 40 °C. The mobile phase flow rate was 0.4 µL/min, and separation was performed using a 265-min gradient consisting of 0–35% mobile phase B over 255 min, followed by 10 min at 90% B. Samples were injected in partial-injection mode and analyzed in technical duplicate.

Mass spectrometric acquisition was performed in positive-ion mode with a capillary voltage of 1450 V, nebuliser pressure of 0.4 pounds per square inch (psi), gas flow rate of 3.0 L/min, and gas temperature of 150 °C. Spectra were acquired over an m/z range of 50–2200 at a scan rate of 8100 m/z/s. HyStar software (version 5.1.8.1; Bruker Daltonik GmbH, Bremen, Germany) was used to define the LC–MS acquisition methods and sample information. The acquired spectra and chromatograms were processed using DataAnalysis software (version 5.3; Bruker Daltonik GmbH, Bremen, Germany), and subsequent data analysis was performed using ProteinScape software (version 4.0.3.315; Bruker Daltonik GmbH, Bremen, Germany).

Protein identification was performed using Mascot Server version 2.5.0 against the Swiss-Prot database, restricted to *Rattus norvegicus*. Database searches allowed up to two missed tryptic cleavage sites, with carbamidomethylation specified as a fixed modification and phosphorylation and oxidation as variable modifications. Monoisotopic masses were used, with peptide mass and MS/MS fragment mass tolerances of ±0.6 Da. Peptide identifications were filtered at a 1% false discovery rate (FDR). Protein identification required at least one peptide with a Mascot score exceeding the Mascot identity score at a significance thresh-

old of $p < 0.05$. The ion score cut-off was set to 15, the peptide rank cut-off to 10, and the minimum peptide length to five amino acid residues. The nanoLC–MS/MS analysis and protein identification were performed according to our previously established protocols [12,20].

2.6 Machine Learning-Based Identification of Discriminating Proteins

To identify proteins with the greatest discriminatory power between diabetic (n = 6) and control (n = 6) animals, a multi-step machine learning workflow was implemented in R (version 4.2) [21,22]. Protein abundance values obtained by LC–MS/MS were assembled into a sample-by-protein matrix, where rows represented individual animals and columns represented quantified proteins. Prior to model development, protein abundances were $\log_2$-transformed and autoscaled (mean-centred and scaled to unit variance).

Three supervised learning algorithms were applied: orthogonal partial least squares discriminant analysis (OPLS-DA), random forest (RF), and support vector machine (SVM). OPLS-DA models were generated using the ropls package [23], random forest models using the randomForest package (ntree = 500) [24], and SVM models using the e1071 [25] and caret packages with a radial basis function (RBF) kernel. Feature selection for SVM was performed using recursive feature elimination (SVM-RFE) implemented within the caret framework [21,22].

The analysis workflow consisted of five consecutive steps. First, classification models were trained using the complete proteomic dataset. Second, model performance was evaluated using leave-one-out cross-validation (LOOCV), where one sample was excluded for testing and the remaining samples were used for model training. This procedure was repeated until each sample had served once as the test sample. Classification performance was assessed using accuracy, F1 score, and Cohen's kappa coefficient. Given the limited sample size, cross-validation and model-specific internal validation procedures were applied to assess model generalisability and the potential risk of overfitting.

Third, model robustness was evaluated. For OPLS-DA, model quality was assessed using the R^2Y coefficient, the Q^2 statistic, and permutation testing employing 100 random permutations of class labels. For random forest, robustness was estimated using the out-of-bag (OOB) error estimate derived from bootstrap aggregation. For SVM, predictive performance was evaluated using LOOCV classification metrics.

Fourth, variable importance was determined independently for each model. In OPLS-DA, variable importance in projection (VIP) scores were used. For random forest, feature importance was quantified using mean decrease in impurity (Gini importance) and mean decrease in accuracy. For SVM, predictors were ranked according to their contribution to classification performance during recursive feature elimination.

Finally, importance scores obtained from all three algorithms were min–max normalized to a common 0–1 scale within each model and subsequently averaged to generate an ensemble importance score. Proteins were ranked according to this score, and the top 20 proteins were selected as the most robust discriminators between diabetic and control groups. These proteins were subsequently subjected to hierarchical clustering, protein–protein interaction and pathway analyses, as well as Gene Ontology (GO) enrichment analysis to further characterise their biological functions.

2.7 AOFA, PRDX3, and PRDX5 Protein Quantification by ELISA

Monoamine oxidase A (AOFA), thioredoxin-dependent peroxide reductase (PRDX3), and peroxiredoxin-5 (PRDX5) protein levels in isolated cardiac mitochondria were determined using commercially available rat-specific ELISA kits (Rat Maoa (Monoamine Oxidase Type A) ELISA Kit, ER0340, FineTest; Rat Thioredoxin-dependent peroxide reductase, mitochondrial (Prdx3) ELISA Kit, RTEB0757, Assay Genie; Rat Peroxiredoxin-5, mitochondrial (Prdx5) ELISA Kit, RTEB0414, Assay Genie) according to the manufacturers' instructions. Mitochondrial samples were normalized to a total protein concentration of 1 µg/µL using the respective sample dilution buffers and subsequently diluted as required to obtain measurements within the assay range. Samples and standards were analyzed in duplicate. Absorbance was measured at 450 nm, and protein concentrations were calculated from the corresponding standard curves. Results were normalized to total mitochondrial protein.

2.8 Statistical Analysis

Data normality was assessed using the Shapiro–Wilk test prior to statistical analysis of metabolic parameters, body weight, and ELISA measurements. Differences in metabolic parameters and body weight between control and diabetic groups were evaluated using an unpaired Student's *t*-test. For ELISA measurements, normally distributed data were analyzed using an unpaired *t*-test with Welch's correction, whereas the Mann–Whitney U test was used when the assumption of normality was not met. Statistical analysis of the ELISA data was performed using GraphPad Prism version 11.1.0 (224) (GraphPad Software, Boston, MA, USA). A p-value < 0.05 was considered statistically significant.

Proteomic data analysis was performed according to the approach previously described by Andelova et al. [20] with some modifications. Proteins with two or more identified peptides were further evaluated by the label-free method of the exponentially modified Protein Abundance Index (emPAI). Differential expression analysis was

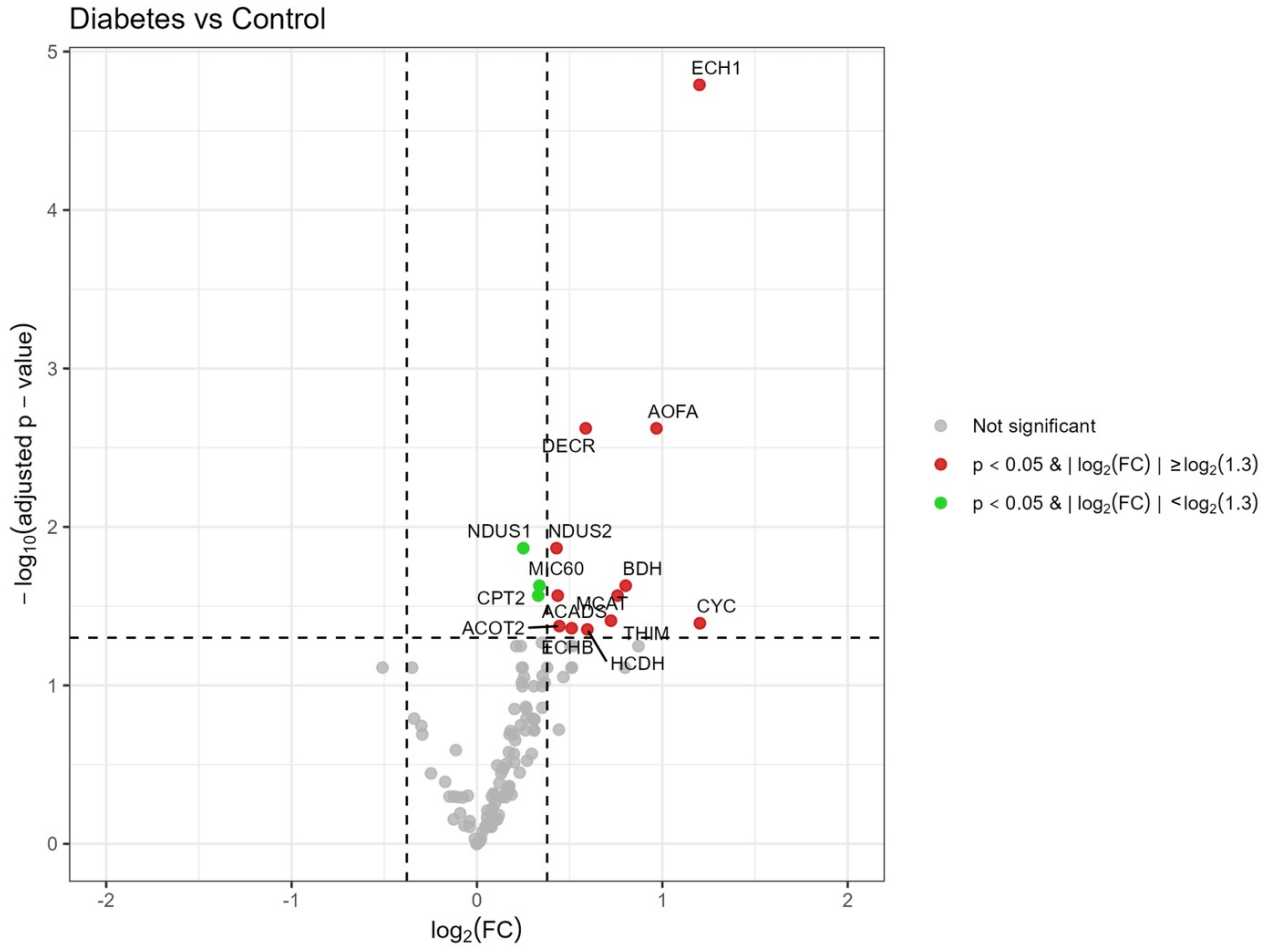

Fig. 1. Volcano plot of differential protein expression between diabetic (D) and control (C) groups. The x-axis represents the $\log_2$ fold-change ($\log_2$FC), where positive values indicate higher protein abundance in the diabetic group and negative values indicate lower protein abundance relative to controls. The y-axis shows statistical significance expressed as $-\log_{10}$ (adjusted *p*-value) following Benjamini–Hochberg correction. The horizontal dashed line indicates the significance threshold ($p_{adjust} < 0.05$), whereas the vertical dashed lines indicate the predefined fold-change threshold ($|\log_2 FC| \geq 0.38$; equivalent to a ≥30% change). Grey dots represent non-significant proteins, green dots represent significantly differentially expressed proteins below the fold-change threshold, and red dots represent significantly differentially expressed proteins exceeding the fold-change threshold. (n = 6 per group).

performed using the *limma* package in R (Bioconductor) [26]. A linear model was fitted to the data, and empirical Bayes moderation was applied to improve variance estimation. *p*-values were adjusted for multiple testing using the Benjamini–Hochberg (BH) method. Proteins with an adjusted *p*-value < 0.05 were considered significantly differentially expressed. Additionally, a fold-change threshold corresponding to a ≥30% change ($|\log_2 FC| \geq 0.38$) was applied. Pearson's correlation coefficient was used for exploratory analysis and visualisation of correlation patterns. Protein interaction maps were created using STRING v12.0 [27]. Gene Ontology (GO) enrichment analysis of the top 20 proteins identified by the combined machine learning model was performed using STRING v12.0 for *Rattus norvegicus*. Biological Process, Molecular Function, and Cellular Component categories were analyzed using the whole-genome background, with FDR <0.05 considered statistically significant. Cytoscape 3.10.1 software [28] was used to edit the protein interaction maps and visualise correlation results. The Kyoto Encyclopedia of Genes and Genomes (KEGG) database was used for pathway mapping and visualisation [29].

3. Results

The diabetic status of the animals was confirmed on day 8 by significant increases in plasma glucose, triacylglycerols, and cholesterol levels, together with a significant decrease in insulin levels compared with age-matched controls (C), as summarised in Table 1 and consistent with our previous findings [5,7,12].

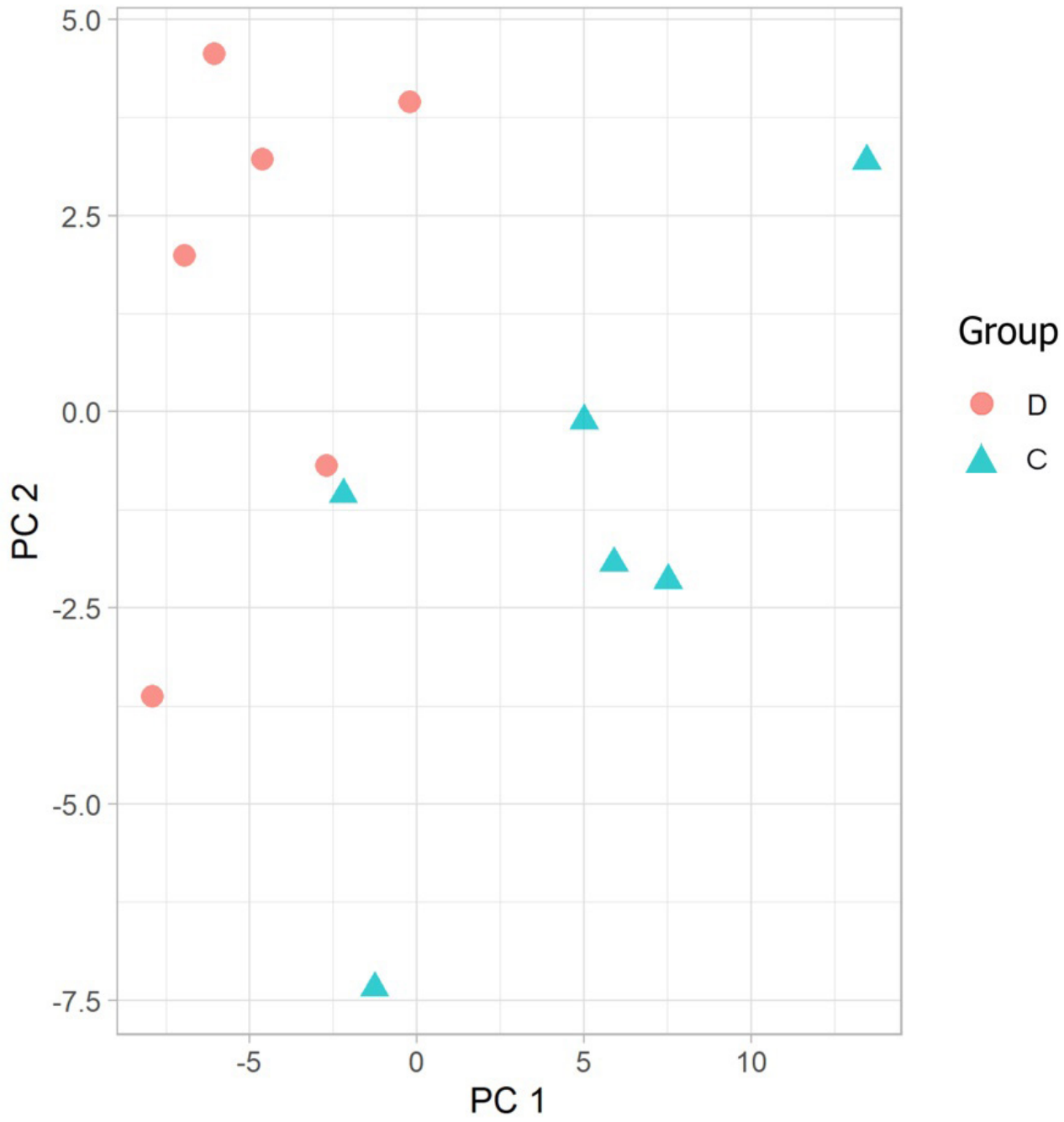

Fig. 2. Principal component analysis (PCA) of proteomic data from diabetic (D) and control (C) groups. Samples are plotted according to the first two principal components (PC1 and PC2). Colours and symbols indicate the predicted group classification based on the combined machine learning model (SVM, random forest, and OPLS-DA). (n = 6 per group).

3.1 Differential Analysis of Proteomic Data

To characterise mitochondrial adaptations associated with acute diabetes (D), LC-MS/MS-based proteomic profiling of isolated cardiac mitochondria was performed. Differential expression analysis of 114 proteins that met the inclusion criteria identified 15 significantly upregulated proteins, of which 12 also exceeded the predefined fold-change threshold. No significantly downregulated proteins were detected. The most statistically significant changes were observed for ECH1 (Δ3,5,Δ2,4-dienoyl-CoA isomerase, $p_{adjust} < 0.001$), AOFA (monoamine oxidase A, $p_{adjust} = 0.003$), and DECR (2,4-dienoyl-CoA reductase, $p_{adjust} = 0.003$). These results are visualised in the volcano plot (Fig. 1), showing a clear predominance of upregulated proteins among the significantly altered proteins. A substantial proportion of the significantly altered proteins

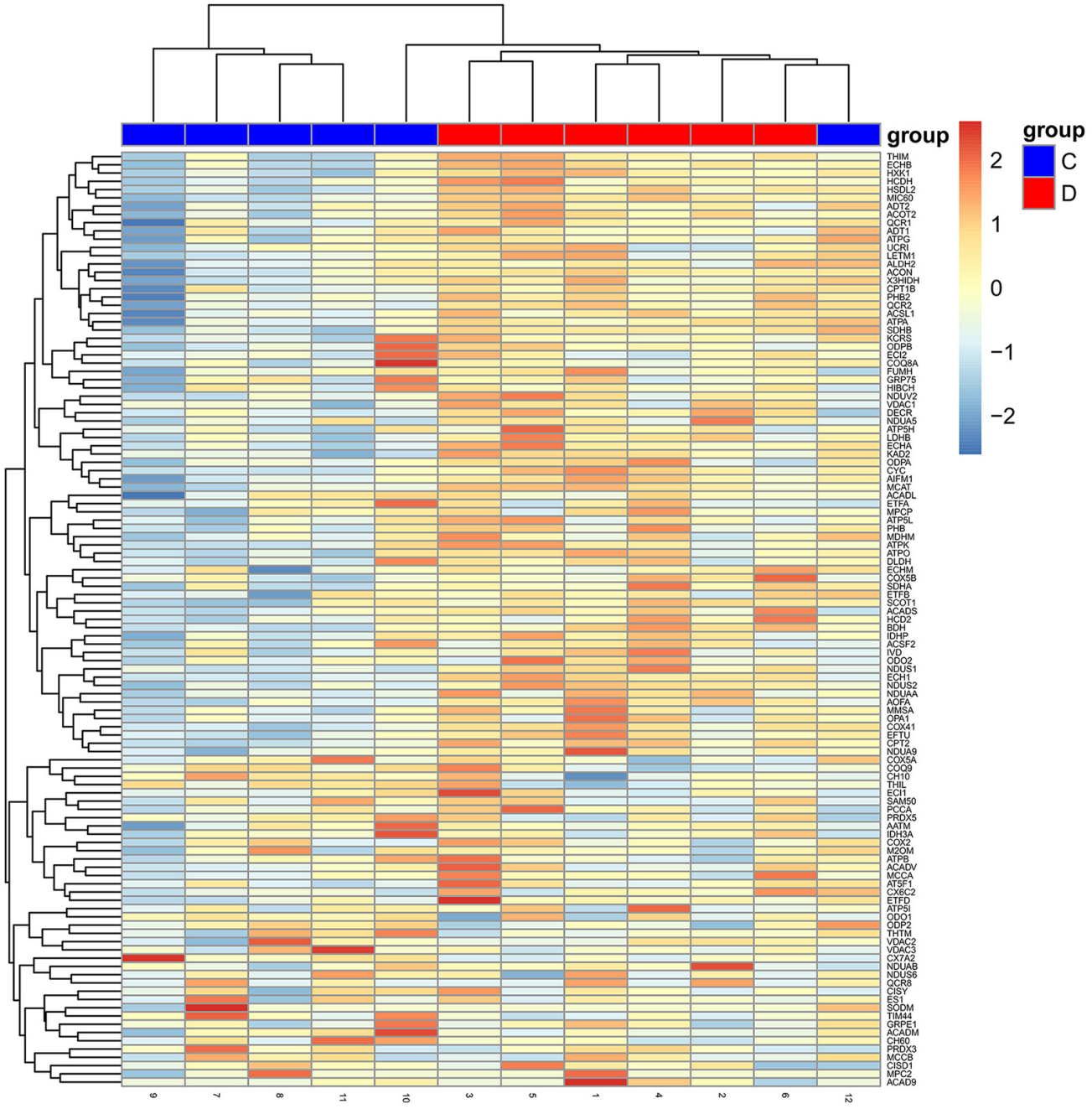

Fig. 3. Hierarchical clustering heat map of proteomic data from diabetic (D) and control (C) groups. Values are presented as row-wise *z*-scores, with red indicating higher and blue indicating lower protein abundance relative to the mean abundance of each protein across all samples. The top dendrogram represents clustering of experimental animals, and the left dendrogram represents clustering of proteins. The coloured bar above the heat map indicates the experimental groups. (n = 6 per group).

was associated with mitochondrial β-oxidation (ACOT2, p_{adjust} = 0.043; ACADS, p_{adjust} = 0.030; MCAT, p_{adjust} = 0.030; THIM, p_{adjust} = 0.041; ECHB, p_{adjust} = 0.046; HCDH, p_{adjust} = 0.049). Other significantly altered proteins included the complex I subunit NDUS2 (NADH dehydrogenase [ubiquinone] iron-sulfur protein 2, p_{adjust} = 0.016), CYC (cytochrome c, p_{adjust} = 0.041), and BDH (D-beta-hydroxybutyrate dehydrogenase, p_{adjust} = 0.026). The remaining three significantly upregulated proteins, which did not exceed the predefined fold-change threshold, were NDUS1 (NADH-ubiquinone oxidoreductase 75 kDa subunit, p_{adjust} = 0.016), MIC60 (MICOS complex subunit Mic60, p_{adjust} = 0.026), and CPT2 (carnitine O-palmitoyltransferase 2, p_{adjust} = 0.030).

3.2 Identification of Key Discriminating Proteins

Classification models were constructed using three different approaches (OPLS-DA, random forest, and

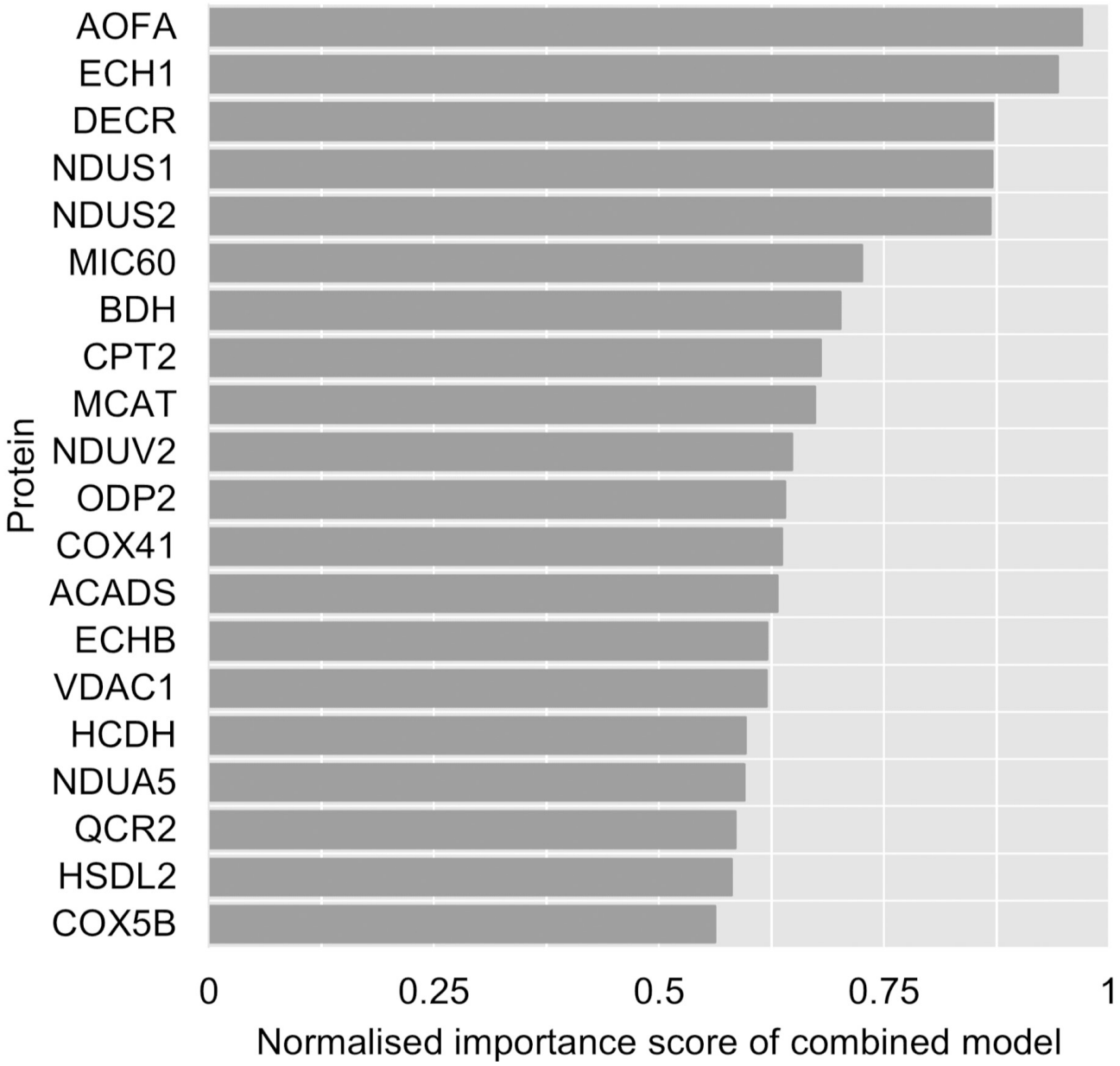

Fig. 4. Normalized ensemble importance scores of the top 20 proteins identified by the combined machine learning model. Importance scores were calculated by integrating the normalized feature importance scores obtained from the OPLS-DA, random forest, and SVM models. Higher scores indicate a greater contribution of individual proteins to the discrimination between diabetic (D) and control (C) groups.

SVM). This approach identified the top 20 proteins that best distinguished diabetic and control groups. Unlike conventional univariate analyses, ML methods account for interdependencies among proteins and enable detection of complex, non-linear relationships within the dataset [30]. To minimise overfitting during model development—particularly given the relatively small sample size compared to the number of parameters—LOOCV, permutation testing, and bootstrapping were applied [31]. The results of LOOCV, as well as bootstrapping and permutation tests for each model, are presented in Table 2. The results of the combined analysis are visualised in Fig. 2. Hierarchical clustering analysis further supported these findings, with the resulting heat map shown in Fig. 3. We focused on the top 20 proteins with the highest ensemble importance scores, which are summarised in Fig. 4. A Venn diagram illustrating the overlap between classifiers (OPLS-DA, random forest, and SVM) is presented in Fig. 5, highlighting shared discriminating proteins across models.

3.3 Functional Analysis of Key Discriminating Proteins

The discriminating proteins were further subjected to Gene Ontology (GO) enrichment and STRING protein–protein interaction analyses. GO enrichment analysis of the

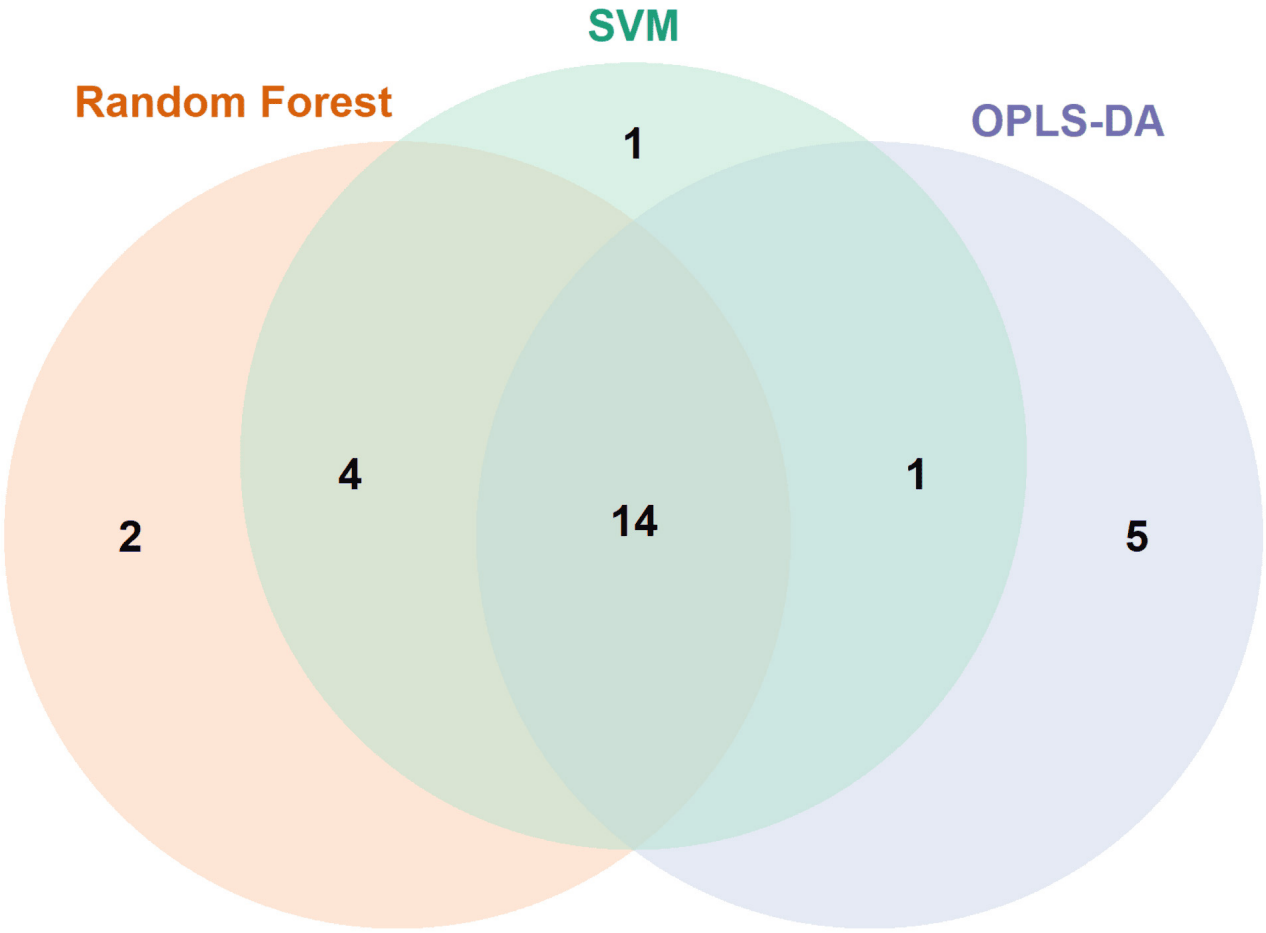

Fig. 5. Venn diagram showing the overlap among the top 20 proteins identified by the combined machine learning model. Proteins were ranked according to their normalized importance scores in the individual OPLS-DA, random forest, and SVM models. Numbers indicate the number of proteins unique to or shared among the three models.

Table 2. Leave-one-out cross-validation, bootstrapping, and permutation testing of classification models.

Model	LOOCV			Bootstrapping/permutation testing
	Accuracy	F1	Cohen's Kappa	
OPLS-DA	0.917	0.923	0.833	$R^2 = 0.978$ ($p_{perm} < 0.05$) $Q^2 = 0.766$ ($p_{perm} < 0.05$)
RF	0.833	0.833	0.667	OOB error estimate: 16.67%
SVM	0.917	0.923	0.833	

LOOCV, leave-one-out cross-validation; OPLS-DA, orthogonal partial least squares discriminant analysis; RF, random forest; SVM, support vector machine; OOB, out-of-bag.

top 20 proteins identified by the combined machine learning model revealed significant enrichment of mitochondrial metabolic processes (Fig. 6). The most strongly enriched Biological Process terms included fatty acid β-oxidation (FDR = 3.01×10^{-7}), cellular respiration (FDR = 9.52×10^{-7}), and respiratory electron transport chain (FDR = 1.16×10^{-6}). Molecular Function analysis showed enrichment of oxidoreductase activity (FDR = 1.15×10^{-6}) and electron transfer activity (FDR = 3.70×10^{-4}), whereas Cellular Component analysis confirmed predominant mitochondrial localisation, particularly within the mitochondrion (FDR = 2.57×10^{-20}) and mitochondrial membrane (FDR = 9.65×10^{-17}). A complete list of enriched GO terms, together with the corresponding enrichment statistics, is provided in **Supplementary Table 1**. STRING network analysis combined with MCL clustering was subsequently performed (Fig. 7). In the comparison between D and C groups, proteins segregated into two main clusters: (1) proteins associated with the citric acid cycle and respiratory electron transport, and (2) proteins involved in fatty acid β-oxidation. As

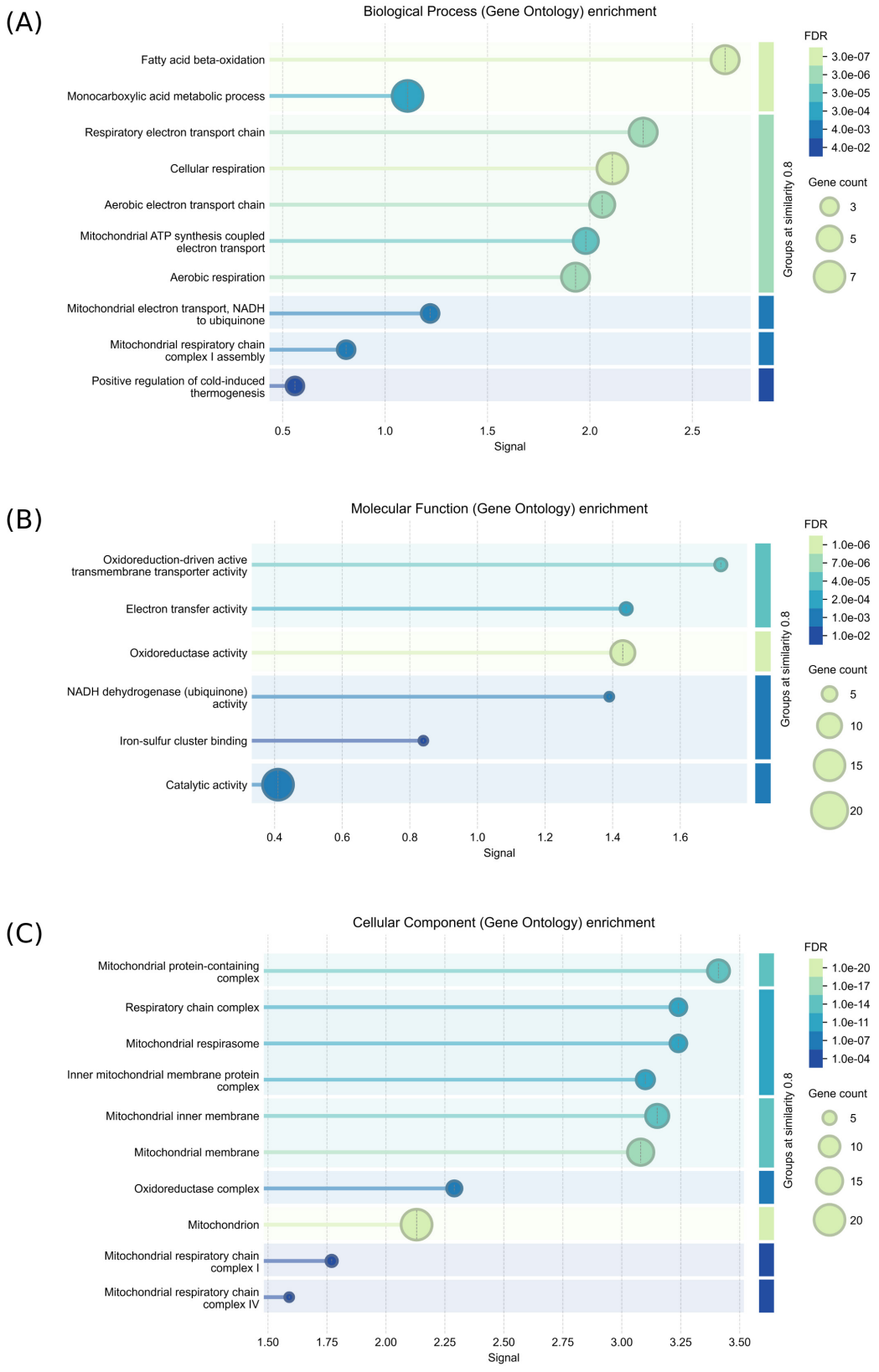

Fig. 6. Gene Ontology (GO) enrichment analysis of the top 20 discriminating proteins identified by the combined machine learning model. Enrichment analysis was performed using STRING and is shown for (A) Biological Process, (B) Molecular Function, and (C) Cellular Component. The x-axis represents the STRING enrichment signal. Bubble size indicates the number of proteins associated with each GO term, and colour represents the false discovery rate (FDR). Functionally related GO terms were grouped at a similarity threshold of 0.8.

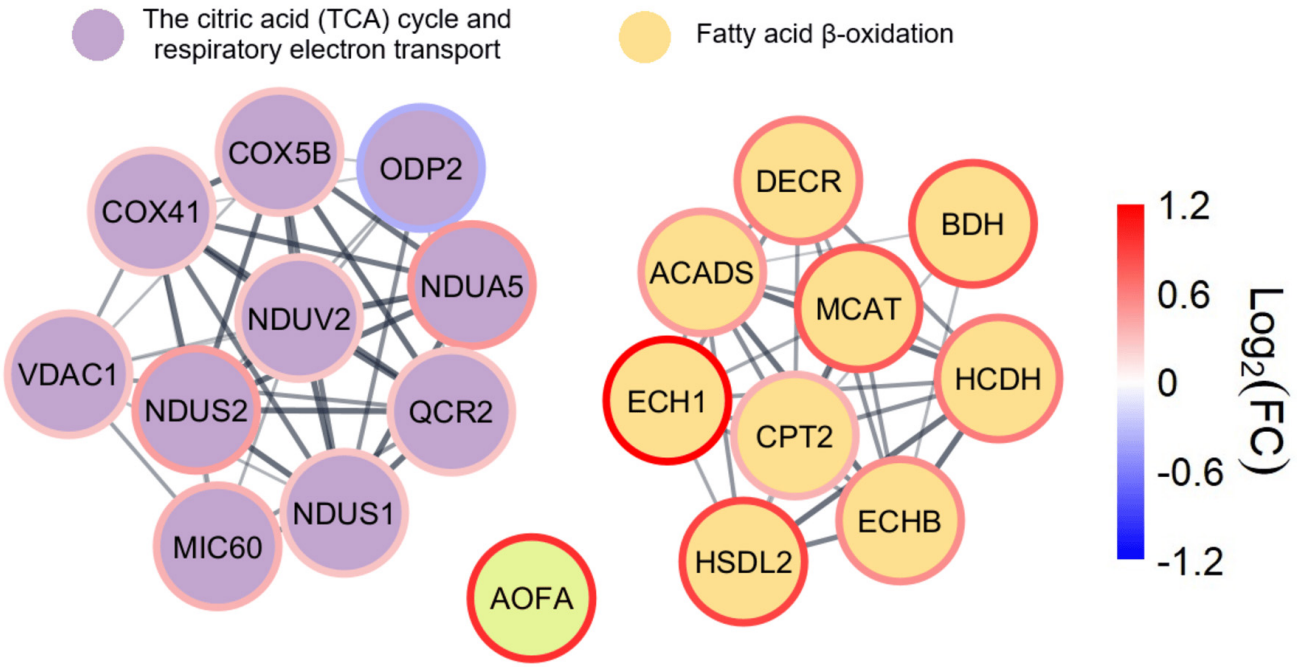

Fig. 7. STRING protein–protein interaction network of the discriminating proteins identified by the combined machine learning model following Markov Cluster Algorithm (MCL) clustering (inflation parameter = 3; interaction score threshold = 0.4). Nodes represent proteins grouped according to their predominant biological function. Edge connectivity represents protein–protein interactions obtained from the STRING database, whereas node border colour indicates the fold-change (log_2FC) in protein abundance in the diabetic (D) group relative to the control (C) group. The network was visualised using Cytoscape. (n = 6 per group).

proteins involved in fatty acid β-oxidation were both statistically significant and consistently identified as discriminating features by the machine learning analysis, they were subsequently mapped onto the KEGG pathway to visualise pathway-level changes (Fig. 8).

3.4 Analysis of Mitochondrial Antioxidant Enzymes and Monoamine Oxidase A

LC-MS/MS-based proteomic analysis revealed a significant upregulation of AOFA in the D group (p_{adjust} = 0.003), while mitochondrial peroxiredoxins (PRDXs) and superoxide dismutase [Mn] (SODM) did not show any significant changes. Fig. 9 illustrates the fold changes of these proteins, whereas Fig. 10 presents the correlation analysis separately for each experimental group. In the diabetic group, a positive correlation was observed between PRDX3 and AOFA (r = 0.636), whereas PRDX5 showed negative correlations with AOFA (r = −0.697) and PRDX3 (r = −0.620) (Fig. 10A). In the control group, a moderate positive correlation was observed between PRDX3 and SODM (r = 0.320), whereas most other correlations were negative, including those between AOFA and PRDX3 (r = −0.420) and SODM and PRDX5 (r = −0.480) (Fig. 10B).

To further characterise these redox-related changes at the protein level, AOFA, PRDX3, and PRDX5 were additionally assessed by ELISA (Fig. 11). AOFA protein levels were significantly increased in cardiac mitochondria from diabetic rats compared with controls (66.83 ± 9.21 vs. 29.65 ± 2.33 ng/mg total protein, respectively; p = 0.002; Fig. 11A), consistent with the increased AOFA abundance detected by LC–MS/MS. In contrast, no significant differences between control and diabetic groups were observed for PRDX3 (184.06 ± 27.90 vs. 193.75 ± 17.39 ng/mg total protein, respectively; p = 0.490; Fig. 11B) or PRDX5 (90.45 ± 6.90 vs. 97.96 ± 7.10 ng/mg total protein, respectively; p = 0.093; Fig. 11C). These findings were consistent with the proteomic analysis, supporting the LC–MS/MS results for all three redox-related proteins examined.

4. Discussion

In our experimental model of acute diabetes, we aimed to characterise the adaptive mechanisms that appear in cardiac mitochondria in response to altered substrate availability and redox imbalance. Several measurable parameters indicated remodelling of mitochondrial function: accumulation of oxidised CoQ_9 along with slowing of electron flow in the respiratory chain [7], and changes in membrane properties such as increased fluidity and lower membrane potential [10]. Along with these changes, protective properties have also been observed, including delayed mPTP opening [12] and smaller infarct size after IRI [4]. In this context, the present study extends our previous functional observations and targeted proteomic analyses by providing a broader molecular-level characterisation of mitochondrial

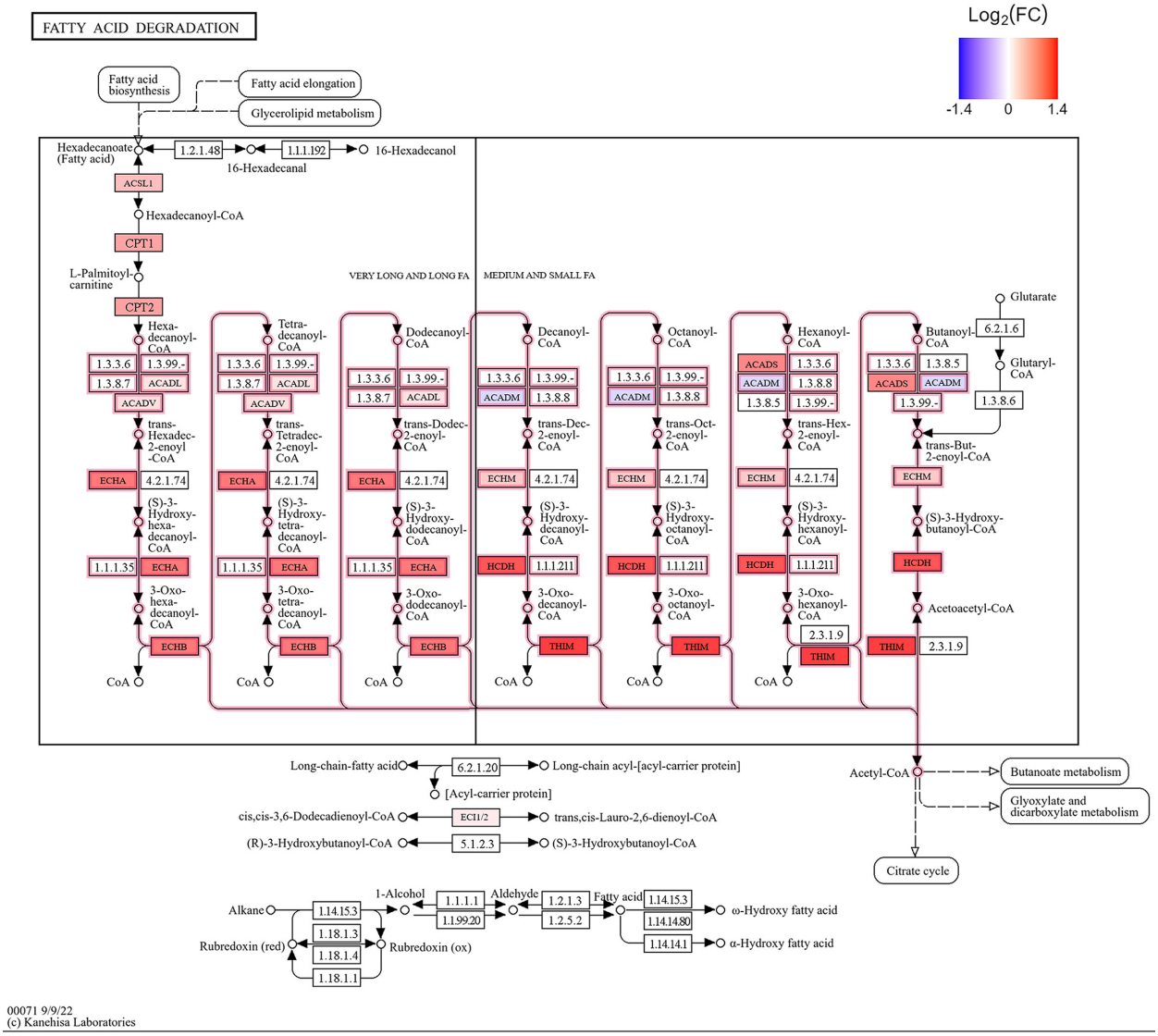

Fig. 8. KEGG pathway map of mitochondrial fatty acid β-oxidation showing differentially expressed proteins in the diabetic (D) group relative to the control (C) group. Proteins identified by LC–MS/MS proteomic analysis are highlighted according to their fold-change (log_2FC), with red indicating upregulation and blue indicating downregulation. The left part of the pathway includes enzymes involved in long-chain fatty acid metabolism (ACSL1, long-chain fatty acid-CoA ligase 1; CPT1/2, carnitine O-palmitoyltransferase 1/2; ACADV, ACADL, very long- and long-chain specific acyl-CoA dehydrogenases; ECHA/B, trifunctional enzyme subunits alpha/beta). The right part shows enzymes involved in medium- and short-chain fatty acid metabolism (ACADM, ACADS, medium- and short-chain specific acyl-CoA dehydrogenases; ECHM, enoyl-CoA hydratase; HCDH, hydroxyacyl-CoA dehydrogenase; THIM, 3-ketoacyl-CoA thiolase).

remodelling during acute diabetes. The integration of LC–MS/MS-based proteomic profiling with differential expression analysis, ML, and functional enrichment approaches enabled the identification and prioritisation of specific proteins and pathways associated with the early diabetic phenotype. This broader analytical framework revealed coordinated changes particularly related to fatty acid β-oxidation, mitochondrial energy metabolism, and redox regulation, providing new molecular insight into the mechanisms potentially underlying the previously observed adaptive phenotype.

Differential expression analysis combined with ML approaches was applied to identify key discriminating proteins. Protein clustering revealed two main clusters corresponding to diabetic (D) and control (C) samples, indicating that diabetes alters the mitochondrial proteomic profile. Notably, 12 of these proteins exhibited statistically significant differences between groups, and 9 showed a fold change greater than 1.3, indicating their potential biological relevance. Importantly, several proteins identified among the top discriminators did not necessarily represent the most statistically significant proteins in the differential

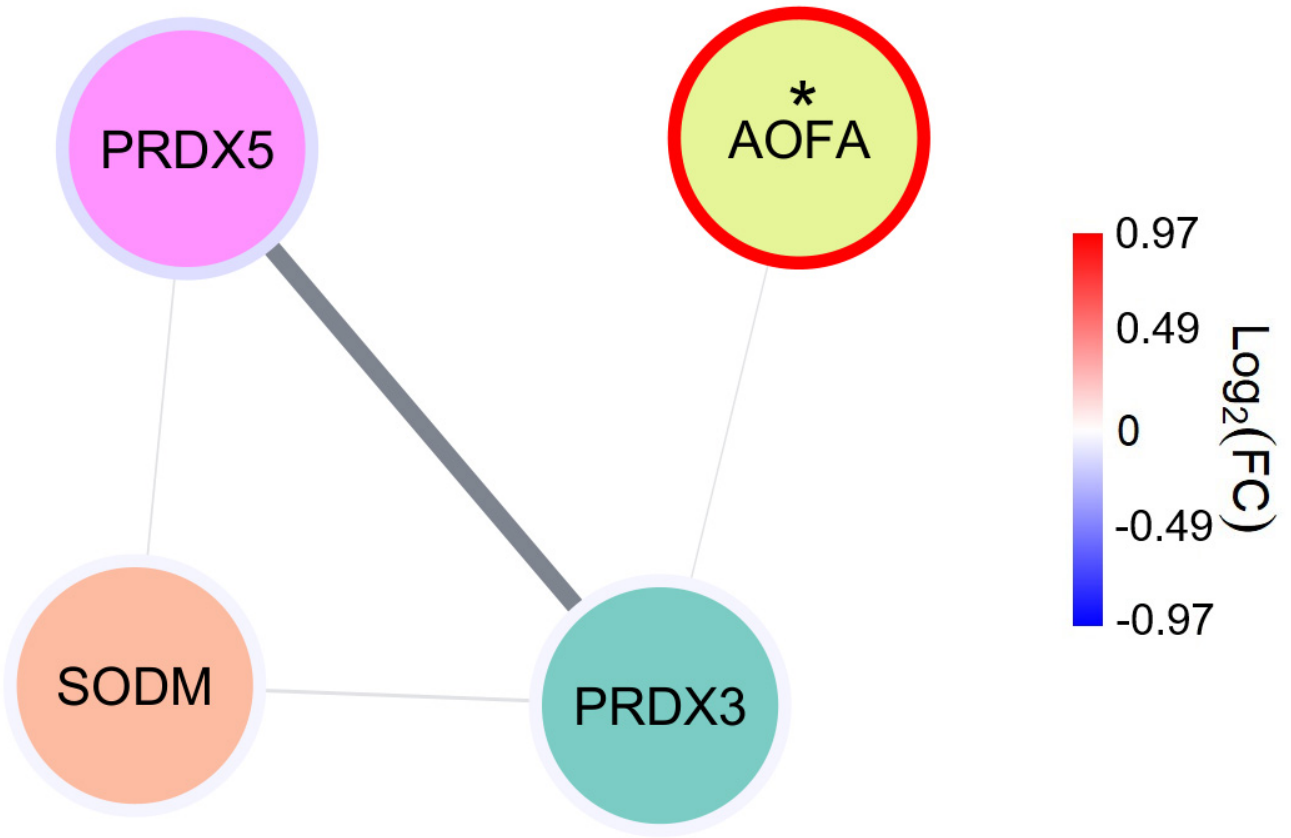

Fig. 9. STRING protein–protein interaction network of antioxidant proteins and monoamine oxidase A (AOFA) identified in cardiac mitochondria. Edge connectivity represents protein–protein interactions obtained from the STRING database, whereas node border colour indicates the fold-change (log_2FC) in protein abundance in the diabetic (D) group relative to the control (C) group. The network was visualised using Cytoscape. An asterisk (*) denotes statistical significance ($p < 0.05$). (n = 6 per group). PRDX3, thioredoxin-dependent peroxide reductase; PRDX5, peroxiredoxin-5; SODM, superoxide dismutase [Mn].

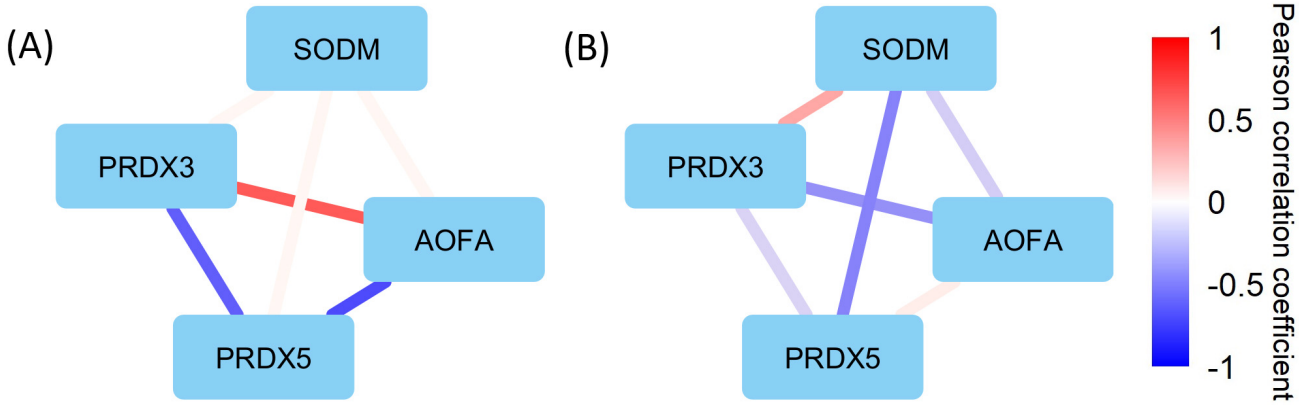

Fig. 10. Protein–protein correlation networks of antioxidant proteins and monoamine oxidase A (AOFA). (A) Diabetic group. (B) Control group. Nodes represent individual proteins, and edges represent Pearson correlation coefficients between protein pairs. Edge colour indicates the direction and strength of the correlation, with positive correlations shown in red and negative correlations in blue. (n = 6 per group). PRDX3, thioredoxin-dependent peroxide reductase; PRDX5, peroxiredoxin-5; SODM, superoxide dismutase [Mn].

expression analysis, indicating that discriminatory importance and statistical significance provide complementary information. The ML approach therefore provided an additional level of prioritisation by identifying proteins contributing to the multivariate separation between diabetic and control mitochondrial proteomes.

Most of the identified proteins were functionally linked to pathways of fatty acid β-oxidation and mitochon-

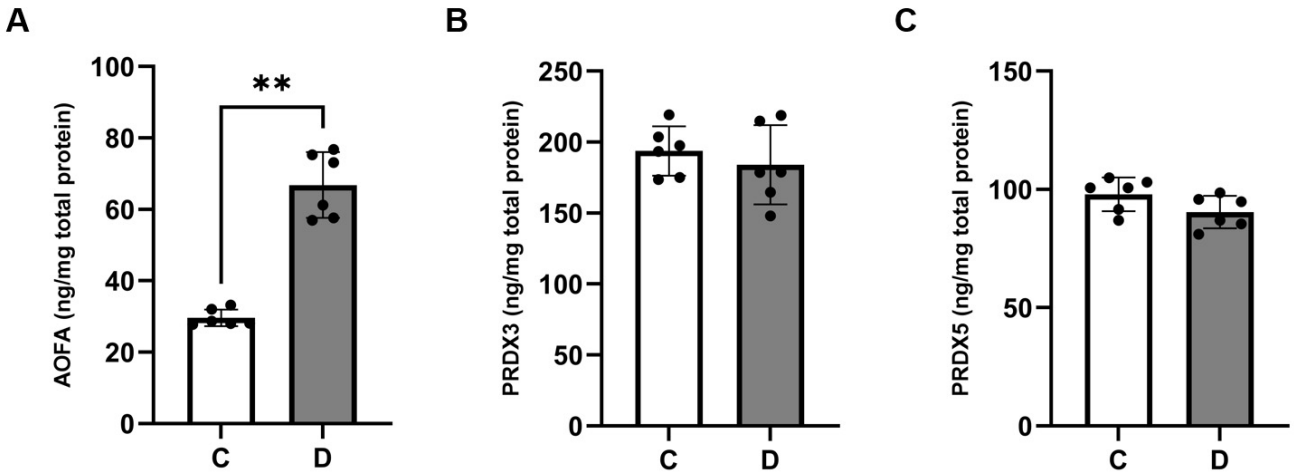

Fig. 11. Protein levels of AOFA, PRDX3, and PRDX5 in cardiac mitochondria of control and diabetic rats determined by ELISA. (A) Monoamine oxidase A (AOFA), (B) thioredoxin-dependent peroxide reductase (PRDX3), and (C) peroxiredoxin-5 (PRDX5). Data are presented as mean ± SD, with individual data points representing individual animals (n = 6 per group). Differences between control (C) and diabetic (D) groups were assessed using an unpaired Student's *t*-test for normally distributed data or the Mann–Whitney U test when the assumption of normality was not met. ** $p < 0.01$ versus control.

drial redox regulation, covering multiple steps of this process, including the metabolism of both saturated and unsaturated fatty acids, which points to a coordinated activation of lipid metabolism. Alongside this, AOFA, which showed the highest discriminatory power across models, represents an important mitochondrial source of ROS and functionally links metabolic activity with redox signalling [32,33]. Based on this functional convergence, we therefore prioritised two interconnected domains—enhanced fatty acid β-oxidation and AOFA-mediated redox modulation—as central mechanisms of mitochondrial adaptation in acute diabetes.

Increased abundance of ECH1 and DECR indicates involvement of the auxiliary β-oxidation pathway [34,35,36]. This finding is consistent with the well-established metabolic shift of the diabetic heart towards increased mitochondrial fatty acid oxidation and reduced glucose oxidation [37]. Although direct studies on ECH1 in cardiomyocytes are limited, its upregulation in skeletal muscle [38] and mitochondrial localisation suggest a similar regulatory role in the heart. In addition, ECH1 has been implicated in promoting fatty acid oxidation while limiting oxidative damage, apoptosis, and inflammatory responses [39]. The role of DECR1 appears more complex, as it has been associated with both protective and pathological processes. It has been shown to attenuate oxidative damage and stabilise mitochondrial function in myocardial infarction [40], whereas its overexpression may enhance fatty acid metabolism and promote excessive ROS production [41]. The presence of CPT2 and MCAT (mitochondrial carnitine/acylcarnitine carrier protein), together with other β-oxidation enzymes, further supports increased transport and processing of fatty acids at the mitochondrial level. Another discriminating protein identified in our dataset, MIC60, is a key regulator of mitochondrial cristae organisation. Its dysfunction has been linked to impaired Ca^{2+} handling, increased sensitivity to mPTP opening, and enhanced cell death signalling [42].

Although only a subset of the 20 discriminating proteins reached statistical significance, Gene Ontology enrichment analysis demonstrated significant enrichment of mitochondrial metabolic processes, particularly fatty acid β-oxidation, cellular respiration, and mitochondrial electron transport. Consistent with these findings, Molecular Function analysis showed enrichment of oxidoreductase and electron transfer activities, while Cellular Component analysis indicated predominant localisation within mitochondrial membranes and respiratory chain complexes. Collectively, this functional convergence supports the biological interpretation of the discriminating proteins as a functionally coherent set reflecting coordinated mitochondrial metabolic remodelling during acute diabetes. In particular, the increased abundance of proteins involved in fatty acid β-oxidation is consistent with previous studies describing a metabolic shift from glucose to fatty acid utilisation in the diabetic heart, leading to enhanced β-oxidation and increased ROS production [43]. While these metabolic alterations are consistent with previous observations in diabetic myocardium, the present study extends these findings by identifying a coordinated mitochondrial protein profile associated with these processes and by prioritising proteins that discriminate between diabetic and control groups. Conversely, the downregulation of ODP2 (dihydrolipoyllysine-residue acetyltransferase component of pyruvate dehydrogenase complex), which participates in the pyruvate dehydrogenase complex linking glycolysis to the Krebs cy-

cle [44], may indicate reduced pyruvate oxidation and a metabolic shift towards alternative energy substrates. Changes in enzymes of intermediate metabolism, including BDH1, suggest that ketone-body metabolism may contribute to the metabolic adaptations observed during acute diabetes [45]. However, as circulating ketone-body levels were not measured, this potential association requires further investigation. The increased abundance of respiratory chain components, particularly complex I proteins (NDUS1 and NDUS2), indicates remodelling of the mitochondrial electron transport machinery. In the context of our previous functional observations showing reduced electron transport efficiency in diabetic mitochondria [7], these proteomic changes may reflect a compensatory response aimed at maintaining mitochondrial energy metabolism rather than an increase in electron transport itself. Together with the observed remodelling of fatty acid β-oxidation-related proteins, these findings support the concept of coordinated metabolic adaptation during the early phase of diabetes [37,46]. Overall, these data point to a coordinated reorganisation of mitochondrial metabolism involving fatty acid β-oxidation-related pathways, the respiratory chain, transport mechanisms, and intermediate metabolism.

A prominent feature of our dataset was the identification of AOFA as one of the top discriminating proteins. AOFA contributes to mitochondrial ROS production by catalysing the oxidative deamination of amines [32,47,48]. SODM represents a major mitochondrial defence against superoxide radicals, and reduced SODM abundance may compromise mitochondrial redox homeostasis [49]. PRDX3 is a major mitochondrial H_2O_2 scavenger and plays an important role in maintaining mitochondrial redox homeostasis, whereas PRDX5 has a broader subcellular distribution and contributes to the detoxification of peroxides in mitochondria and other cellular compartments [33]. Importantly, independent protein-level assessment by ELISA confirmed a significant increase in AOFA in diabetic cardiac mitochondria, consistent with the LC–MS/MS findings. In contrast, PRDX3 and PRDX5 showed no significant differences between groups by ELISA, in agreement with their proteomic profiles. This concordance provides additional support for the redox-related protein changes identified by the proteomic analysis, particularly the prominent increase in AOFA. Although peroxiredoxins did not exhibit increased expression in the diabetic group, their observed correlations with AOFA suggest a potential functional relationship between AOFA-associated ROS production and mitochondrial peroxide defence. This relationship may reflect a tightly regulated redox balance in which increased ROS act not only as damaging agents but also as signalling molecules that trigger adaptive responses [50]. Importantly, despite indications of increased ROS generation, previous studies have shown that mitochondrial membrane fluidity remains preserved in the early phase of diabetes [9,10]. This supports the concept that ROS in this context may contribute to signalling functions rather than solely causing irreversible damage, thereby participating in the modulation of mitochondrial and cellular processes [5,12].

Overall, our results demonstrate that acute diabetes is associated with early remodelling of the mitochondrial proteome, characterised by enhanced fatty acid metabolism, modulation of the electron transport chain, and activation of redox-related pathways. These changes likely represent adaptive mechanisms underlying the observed cardioprotective phenotype. Our data identify AOFA and key metabolic proteins as central components of this response and highlight mitochondrial proteomic reprogramming as a potential contributor to adaptive and compensatory mechanisms in the early phase of diabetes.

5. Study Limitations and Future Directions

The present study was primarily designed as an exploratory proteomic investigation to characterise mitochondrial adaptations associated with acute diabetes and to identify candidate proteins and biological pathways for subsequent targeted investigation. Given the sample size (n = 6 per group), validation of the identified discriminating proteins in independent experimental datasets would provide additional support for their reproducibility. In the present analysis, cross-validation and model-specific internal validation procedures were applied to assess model generalisability and minimise the potential risk of overfitting.

Complementary targeted and metabolic analyses may provide further insight into the functional significance of the observed mitochondrial adaptations. In the present study, independent protein-level assessment by ELISA provided additional support for the proteomic findings for AOFA, PRDX3, and PRDX5, including confirmation of the prominent increase in AOFA in diabetic cardiac mitochondria. Further targeted investigation of other key candidate proteins, particularly ECH1 and DECR, using complementary protein- and gene-expression approaches would extend the molecular characterisation of the identified adaptive response. Additional metabolic analyses, including assessment of relevant circulating metabolites such as ketone bodies, may further clarify the metabolic context of the identified proteomic changes. Such complementary approaches may provide a more comprehensive understanding of the early mitochondrial response to diabetes.

6. Conclusions

The present study demonstrates that acute diabetes induces a distinct mitochondrial proteomic remodelling in the heart, characterised by increased expression of AOFA and coordinated upregulation of proteins involved in fatty acid β-oxidation and the electron transport chain. These changes reflect a shift towards enhanced lipid utilisation and altered mitochondrial energy metabolism. In parallel, modulation of redox-related pathways suggests that ROS

act as signalling mediators contributing to mitochondrial adaptation rather than solely promoting cellular damage. Together, these findings indicate that the early phase of diabetes is associated with targeted mitochondrial reprogramming that supports the maintenance of mitochondrial function under increased energetic and oxidative load. Overall, this study supports the concept that early mitochondrial metabolic adaptation represents a functionally relevant response in the diabetic heart and provides a basis for future targeted investigation of the identified proteins and pathways.

Abbreviations

ACAD, acyl-CoA dehydrogenases; ACSL1, long-chain fatty acid-CoA ligase 1; AOFA, monoamine oxidase A; BDH, D-beta-hydroxybutyrate dehydrogenase; β-oxidation, fatty acid β-oxidation; C, control group; CoQ9, coenzyme Q9; CPT1/2, carnitine O-palmitoyltransferase 1/2; CYC, cytochrome c; D, diabetic group; DECR, 2,4-dienoyl-CoA reductase; ECHA/B, trifunctional enzyme subunits alpha/beta; ECH1, Δ3,5,Δ2,4-dienoyl-CoA isomerase; ECHM, enoyl-CoA hydratase; HCDH, hydroxyacyl-CoA dehydrogenase; KEGG, Kyoto Encyclopedia of Genes and Genomes; LC-MS, liquid chromatography–mass spectrometry; LC-MS/MS, liquid chromatography–tandem mass spectrometry; LOOCV, leave-one-out cross-validation; MIC60, MICOS complex subunit Mic60; ML, machine learning; mPTP, mitochondrial permeability transition pore; NADH/NAD^+, nicotinamide adenine dinucleotide, reduced/oxidised form; NDUS1, NADH-ubiquinone oxidoreductase 75 kDa subunit; NDUS2, NADH dehydrogenase [ubiquinone] iron-sulfur protein 2; ODP2, dihydrolipoyllysine-residue acetyltransferase component of pyruvate dehydrogenase complex; OOB, out-of-bag; OPLS-DA, orthogonal partial least squares discriminant analysis; PCA, principal component analysis; PRDX, peroxiredoxin; PRDX3, thioredoxin-dependent peroxide reductase; PRDX5, peroxiredoxin-5; RBF, radial basis function; RF, random forest; ROS, reactive oxygen species; SODM, superoxide dismutase [Mn]; SVM, support vector machine; THIM, 3-ketoacyl-CoA thiolase; VIP, variable importance in projection.

Availability of Data and Materials

The datasets generated and analyzed during the current study are available in the Zenodo repository, https://doi.org/10.5281/zenodo.19341203.

Author Contributions

Conceptualization, DJ, MF, NA, IW and TR; methodology, MF, NA, DJ, IW, SP and MZ; software, MF and MZ; resources, NA and VF; investigation, NA, DJ, MF and VF; validation, NA, DJ, MF; formal analysis, DJ, NA and MZ; data curation, NA, DJ and MF; writing—original draft preparation, MF, MZ, NA and DJ; writing—review and editing, MF, NA, IW and TR; visualization, NA, DJ, MZ and SP; supervision, MF; project administration, MF, NA; funding acquisition, MF, NA and TR. All authors reviewed and approved the final manuscript. All authors contributed to editorial changes in the manuscript. All authors have participated sufficiently in the work and agreed to be accountable for all aspects of the work.

Ethics Approval and Consent to Participate

Animal experiments were approved by the Animal Health and Animal Welfare Division of the State Veterinary and Food Administration of the Slovak Republic (permit No. Ro 3754/18-221/3). All procedures were performed in accordance with the Principles of Laboratory Animal Care established by the Ethical Committee of the Centre of Experimental Medicine of the Slovak Academy of Sciences (CEM SAS) and complied with Directive 2010/63/EU on the protection of animals used for scientific purposes. The study was reported in accordance with the ARRIVE guidelines.

Acknowledgment

We are deeply grateful to the anonymous peer reviewers for their insightful comments and constructive suggestions, which have significantly enhanced the quality and presentation of this work.

Funding

This work was funded by VEGA SR grant No. 2/0016/23, Slovak Research and Development Agency grants APVV-22-0264 and APVV-19-0540, and EU NextGenerationEU through the Recovery and Resilience Plan for Slovakia under the project No. 09I03-03-V04-00437.

Conflicts of Interest

The authors declare no conflicts of interest.

Declaration of AI and AI-Assisted Technologies in the Writing Process

During the preparation of this work, the authors used ChatGPT (OpenAI) to assist with spelling and grammar. After using this tool, the authors reviewed and edited the content as needed and take full responsibility for the content of the publication.

Supplementary Material

Supplementary material associated with this article can be found, in the online version, at https://doi.org/10.31083/FBL55463.

References

[1] Yang HM. Mitochondrial Dysfunction in Cardiovascular Diseases. International Journal of Molecular Sciences. 2025; 26: 1917. https://doi.org/10.3390/ijms26051917

[2] Pagliaro P, Alloatti G, Penna C. Cardioprotection Reloaded: Reflections on 40 Years of Research. Antioxidants (Basel, Switzerland). 2025; 14: 889. https://doi.org/10.3390/antiox14070889

[3] Korkmaz-Icöz S, Lehner A, Li S, Vater A, Radovits T, Hegedűs P, et al. Mild Type 2 Diabetes Mellitus Reduces the Susceptibility of the Heart to Ischemia/Reperfusion Injury: Identification of Underlying Gene Expression Changes. Journal of Diabetes Research. 2015; 2015: 396414. https://doi.org/10.1155/2015/396414

[4] Kondratieva DS, Afanasiev SA, Muslimova EF. Diabetes mellitus—metabolic preconditioning in protecting the heart from ischemic damage? Diabetes Mellitus. 2022; 25: 548–555. https://doi.org/10.14341/DM12933

[5] Ferko M, Kancirová I, Jašová M, Waczulíková I, Čarnická S, Kucharská J, et al. Participation of heart mitochondria in myocardial protection against ischemia/reperfusion injury: benefit effects of short-term adaptation processes. Physiological Research. 2015; 64: S617–S625. https://doi.org/10.33549/physiolres.933218

[6] Penna C, Andreadou I, Aragno M, Beauloye C, Bertrand L, Lazou A, et al. Effect of hyperglycaemia and diabetes on acute myocardial ischaemia-reperfusion injury and cardioprotection by ischaemic conditioning protocols. British Journal of Pharmacology. 2020; 177: 5312–5335. https://doi.org/10.1111/bph.14993

[7] Ferko M, Gvozdjaková A, Kucharská J, Mujkosová J, Waczulíková I, Styk J, et al. Functional remodeling of heart mitochondria in acute diabetes: interrelationships between damage, endogenous protection and adaptation. General Physiology and Biophysics. 2006; 25: 397–413.

[8] Kancirová I, Jašová M, Muráriková M, Sumbalová Z, Uličná O, Ravingerová T, et al. Cardioprotection induced by remote ischemic preconditioning preserves the mitochondrial respiratory function in acute diabetic myocardium. Physiological Research. 2016; 65: S611–S619. https://doi.org/10.33549/physiolres.933533

[9] Ferko M, Habodászová D, Waczulíková I, Mujkošová J, Kucharská J, Šikurová L, et al. Endogenous protective mechanisms in remodeling of rat heart mitochondrial membranes in the acute phase of streptozotocin-induced diabetes. Physiological Research. 2008; 57: S67–S73. https://doi.org/10.33549/physiolres.931554

[10] Ziegelhöffer A, Waczulíková I, Ferko M, Šikurová L, Mujkošová J, Ravingerová T. Involvement of membrane fluidity in endogenous protective processes running on subcellular membrane systems of the rat heart. Physiological Research. 2012; 61: S11–S21. https://doi.org/10.33549/physiolres.932361

[11] Lu X, Kwong JQ, Molkentin JD, Bers DM. Individual Cardiac Mitochondria Undergo Rare Transient Permeability Transition Pore Openings. Circulation Research. 2016; 118: 834–841. https://doi.org/10.1161/CIRCRESAHA.115.308093

[12] Andelova N, Waczulikova I, Kunstek L, Talian I, Ravingerova T, Jasova M, et al. Dichloroacetate as a metabolic modulator of heart mitochondrial proteome under conditions of reduced oxygen utilization. Scientific Reports. 2022; 12: 16348. https://doi.org/10.1038/s41598-022-20696-5

[13] Jašová M, Kancirová I, Waczulíková I, Ferko M. Mitochondria as a target of cardioprotection in models of preconditioning. Journal of Bioenergetics and Biomembranes. 2017; 49: 357–368. https://doi.org/10.1007/s10863-017-9720-1

[14] Song J, Yang X, Yan LJ. Role of pseudohypoxia in the pathogenesis of type 2 diabetes. Hypoxia (Auckland, N.Z.). 2019; 7: 33–40. https://doi.org/10.2147/HP.S202775

[15] Krediet RT, Parikova A. Glucose-induced pseudohypoxia and advanced glycosylation end products explain peritoneal damage in long-term peritoneal dialysis. Peritoneal Dialysis International : Journal of the International Society for Peritoneal Dialysis. 2024; 44: 6–15. https://doi.org/10.1177/08968608231196033

[16] Ravingerová T, Neckár J, Kolár F. Ischemic tolerance of rat hearts in acute and chronic phases of experimental diabetes. Molecular and Cellular Biochemistry. 2003; 249: 167–174. https://doi.org/10.1023/a:1024751109196

[17] Ziegelhöffer A, Waczulíková I, Ferko M, Kincelová D, Ziegelhöffer B, Ravingerová T, et al. Calcium signaling-mediated endogenous protection of cell energetics in the acutely diabetic myocardium. Canadian Journal of Physiology and Pharmacology. 2009; 87: 1083–1094. https://doi.org/10.1139/Y09-108

[18] Bradford MM. A rapid and sensitive method for the quantitation of microgram quantities of protein utilizing the principle of protein-dye binding. Analytical Biochemistry. 1976; 72: 248–254. https://doi.org/10.1016/0003-2697(76)90527-3

[19] Kancirová I, Jašová M, Waczulíková I, Ravingerová T, Ziegelhöffer A, Ferko M. Effect of antihypertensive agents - captopril and nifedipine - on the functional properties of rat heart mitochondria. Iranian Journal of Basic Medical Sciences. 2016; 19: 615–623.

[20] Andelova N, Waczulikova I, Talian I, Sykora M, Ferko M. mPTP Proteins Regulated by Streptozotocin-Induced Diabetes Mellitus Are Effectively Involved in the Processes of Maintaining Myocardial Metabolic Adaptation. International Journal of Molecular Sciences. 2020; 21: 2622. https://doi.org/10.3390/ijms21072622

[21] R Core Team. R: a language and environment for statistical computing [Computer software]. R Foundation for Statistical Computing: Vienna, Austria. 2023. Available at: https://www.R-project.org/ (Accessed: 29 June 2026).

[22] Kuhn M. Building predictive models in R using the caret package. Journal of statistical software. 2008; 28: 1–26. https://doi.org/10.18637/jss.v028.i05

[23] Thévenot EA, Roux A, Xu Y, Ezan E, Junot C. Analysis of the Human Adult Urinary Metabolome Variations with Age, Body Mass Index, and Gender by Implementing a Comprehensive Workflow for Univariate and OPLS Statistical Analyses. Journal of Proteome Research. 2015; 14: 3322–3335. https://doi.org/10.1021/acs.jproteome.5b00354

[24] Liaw A, Wiener M. Classification and regression by randomForest. R News. 2002. Available at: https://CRAN.R-project.org/doc/Rnews/ (Accessed: 29 June 2026).

[25] Meyer D, Dimitriadou E, Hornik K, Weingessel A, Leisch F. e1071: Misc Functions of the Department of Statistics, Probability Theory Group (Formerly: E1071), TU Wien (version 1.7-16) [Computer software]. Comprehensive R Archive Network (CRAN). 2024. https://CRAN.R-project.org/package=e1071

[26] Ritchie ME, Phipson B, Wu D, Hu Y, Law CW, Shi W, et al. limma powers differential expression analyses for RNA-sequencing and microarray studies. Nucleic Acids Research. 2015; 43: e47. https://doi.org/10.1093/nar/gkv007

[27] Szklarczyk D, Kirsch R, Koutrouli M, Nastou K, Mehryary F, Hachilif R, et al. The STRING database in 2023: protein-protein association networks and functional enrichment analyses for any sequenced genome of interest. Nucleic Acids Research. 2023; 51: D638–D646. https://doi.org/10.1093/nar/gkac1000

[28] Doncheva NT, Morris JH, Gorodkin J, Jensen LJ. Cytoscape StringApp: Network Analysis and Visualization of Proteomics Data. Journal of Proteome Research. 2019; 18: 623–632. https://doi.org/10.1021/acs.jproteome.8b00702

[29] Kanehisa M, Furumichi M, Sato Y, Kawashima M, Ishiguro-Watanabe M. KEGG for taxonomy-based analysis of pathways

and genomes. Nucleic Acids Research. 2023; 51: D587–D592. https://doi.org/10.1093/nar/gkac963

[30] Acharya D, Mukhopadhyay A. A comprehensive review of machine learning techniques for multi-omics data integration: challenges and applications in precision oncology. Briefings in Functional Genomics. 2024; 23: 549–560. https://doi.org/10.1093/bfgp/elae013

[31] Rodríguez-Pérez R, Fernández L, Marco S. Overoptimism in cross-validation when using partial least squares-discriminant analysis for omics data: a systematic study. Analytical and Bioanalytical Chemistry. 2018; 410: 5981–5992. https://doi.org/10.1007/s00216-018-1217-1

[32] Kaludercic N, Arusei RJ, Di Lisa F. Recent advances on the role of monoamine oxidases in cardiac pathophysiology. Basic Research in Cardiology. 2023; 118: 41. https://doi.org/10.1007/s00395-023-01012-2

[33] Ferko M, Alanova P, Janko D, Opletalova B, Andelova N. Mitochondrial Peroxiredoxins and Monoamine Oxidase-A: Dynamic Regulators of ROS Signaling in Cardioprotection. Physiological Research. 2024; 73: 887–900. https://doi.org/10.33549/physiolres.935513

[34] Zhang D, Liang X, He XY, Alipui OD, Yang SY, Schulz H. Delta 3,5,delta 2,4-dienoyl-CoA isomerase is a multifunctional isomerase. A structural and mechanistic study. The Journal of Biological Chemistry. 2001; 276: 13622–13627. https://doi.org/10.1074/jbc.M011315200

[35] Houten SM, Wanders RJA. A general introduction to the biochemistry of mitochondrial fatty acid β-oxidation. Journal of Inherited Metabolic Disease. 2010; 33: 469–477. https://doi.org/10.1007/s10545-010-9061-2

[36] Panov AV. The Structure of the Cardiac Mitochondria Respirasome Is Adapted for the β-Oxidation of Fatty Acids. International Journal of Molecular Sciences. 2024; 25: 2410. https://doi.org/10.3390/ijms25042410

[37] Panwar A, Malik SO, Adib M, Lopaschuk GD. Cardiac energy metabolism in diabetes: emerging therapeutic targets and clinical implications. American Journal of Physiology. Heart and Circulatory Physiology. 2025; 328: H1089–H1112. https://doi.org/10.1152/ajpheart.00615.2024

[38] Fiorentino TV, Monroy A, Kamath S, Sotero R, Cas MD, Daniele G, et al. Pioglitazone corrects dysregulation of skeletal muscle mitochondrial proteins involved in ATP synthesis in type 2 diabetes. Metabolism: Clinical and Experimental. 2021; 114: 154416. https://doi.org/10.1016/j.metabol.2020.154416

[39] Miao Y, Yan L, Cao H, Jiao X, Shao F. The Mitochondrial Metabolism Gene ECH1 Was Identified as a Novel Biomarker for Diabetic Nephropathy: Using Bioinformatics Analysis and Experimental Confirmation. Diabetes, Metabolic Syndrome and Obesity : Targets and Therapy. 2025; 18: 1087–1098. https://doi.org/10.2147/DMSO.S494644

[40] Duan Z, Huang Z, Lei W, Zhang K, Xie W, Jin H, et al. Bone Morphogenetic Protein 9 Protects Against Myocardial Infarction by Improving Lymphatic Drainage Function and Triggering DECR1-Mediated Mitochondrial Bioenergetics. Circulation. 2024; 150: 1684–1701. https://doi.org/10.1161/CIRCULATIONAHA.123.065935

[41] Tian J, He Q, Li N, Sun Y, Zhang A, Wang H. FTO-Mediated m6A Demethylation of MZF1 Regulates DECR1 to Promote Fatty Acid Oxidation and Exacerbate Myocardial Ischemia/Reperfusion Injury : FTO-Mediated m6A Demethylation of MZF1 Enhances Fatty Acid Oxidation and Aggravates Myocardial I/R Injury. Biochemical Genetics. 2026; 64: 4353–4374. https://doi.org/10.1007/s10528-025-11251-8

[42] Khan MS, Nasiripour S, Oyarzabal M, Banerjee S, Sharma K, Bhat MA, et al. Mic60/Mitofilin inhibitor, Miclxin, induces rat H9C2 cardiomyoblast death by inhibiting the removal of damaged mitochondria. American Journal of Translational Research. 2025; 17: 6743–6754. https://doi.org/10.62347/UPML8062

[43] Bugger H, Abel ED. Mitochondria in the diabetic heart. Cardiovascular Research. 2010; 88: 229–240. https://doi.org/10.1093/cvr/cvq239

[44] Stacpoole PW, McCall CE. The pyruvate dehydrogenase complex: Life's essential, vulnerable and druggable energy homeostat. Mitochondrion. 2023; 70: 59–102. https://doi.org/10.1016/j.mito.2023.02.007

[45] Wan SR, Teng FY, Fan W, Xu BT, Li XY, Tan XZ, et al. BDH1-mediated βOHB metabolism ameliorates diabetic kidney disease by activation of NRF2-mediated antioxidative pathway. Aging. 2023; 15: 13384–13410. https://doi.org/10.18632/aging.205248

[46] Liu S, Liu J, Wang Y, Deng F, Deng Z. Oxidative Stress: Signaling Pathways, Biological Functions, and Disease. MedComm. 2025; 6: e70268. https://doi.org/10.1002/mco2.70268

[47] Sun Y, Lu Y, Saredy J, Wang X, Drummer Iv C, Shao Y, et al. ROS systems are a new integrated network for sensing homeostasis and alarming stresses in organelle metabolic processes. Redox Biology. 2020; 37: 101696. https://doi.org/10.1016/j.redox.2020.101696

[48] Schulz R, Schlüter KD. Importance of Mitochondria in Cardiac Pathologies: Focus on Uncoupling Proteins and Monoamine Oxidases. International Journal of Molecular Sciences. 2023; 24: 6459. https://doi.org/10.3390/ijms24076459

[49] Murphy E, Liu JC. Mitochondrial calcium and reactive oxygen species in cardiovascular disease. Cardiovascular Research. 2023; 119: 1105–1116. https://doi.org/10.1093/cvr/cvac134

[50] Sandhu JK, Sodja C, Ribecco-Lutkiewicz M, Wu YT, Ma YS, Wei YH, et al. Effects of Tolerance-Induced Preconditioning on Mitochondrial Biogenesis in Undifferentiated and Differentiated Neuronal Cells. Frontiers in Bioscience (Landmark Edition). 2022; 27: 115. https://doi.org/10.31083/j.fbl2704115